

RECONSTRUCTION OF SPHERICAL TORUS EQUILIBRIA IN ABSENCE OF MAGNETIC MEASUREMENTS IN THE CENTRAL CAVITY

F. ALLADIO, P. MICOZZI
Associazione Euratom-ENEA sulla Fusione,
Centro Ricerche Frascati,
Frascati, Rome,
Italy

ABSTRACT. Magnetic measurements alone on spherical tori should allow a very good separation of the poloidal beta β_p from the internal self-inductance $l_i/2$ and should even permit an accurate estimate of the current density j_ϕ profile. However, the reduced space allowed for magnetic sensors near the central conductor in a spherical tokamak, and the possibility of producing flux core spheromak configurations without a central conductor, could imply that magnetic probes are not present in the cavity of the spherical torus. The fluxes and fields of a variety of calculated spherical torus configurations, all endowed with a single or double null separatrix, are analysed in terms of spherical multipolar moments obtained from simulated magnetic measurements located only upon a sphere surrounding the spherical plasma. The solution to the problem of the absence of magnetic measurements in the cavity of the spherical torus is to fix from non-magnetic measurements (e.g., spectroscopy) the plasma inboard boundary r_{in} on the equatorial plane. This constraint is added to the constraints of matching the spherical multipolar expansion in an iterative solution of the Grad-Shafranov equation, on the basis of a spherical geometry. The convergence of the spherical reconstructive equilibrium code is extremely fast and gives an error on the total plasma current I_p of less than 1% at an aspect ratio $A = 1.2$, an error on the position of the plasma boundary of less than 2% of the radius of the plasma sphere, an error on β_p of at most 15% and, finally, the j_ϕ profile is extremely well reconstructed in peaked, flat and even hollow cases. The effect of an uncertainty $\pm \delta r_{in}$ upon the spectroscopic identification of the plasma inboard boundary on the equatorial plane r_{in} is assessed.

1. INTRODUCTION

The spherical torus, also known as the low aspect ratio tokamak (LART), with an aspect ratio $A = R/a < 2$, is a fusion relevant configuration, for a number of reasons [1-3]. Configurations with high plasma current at low toroidal field can be produced by very simple poloidal and toroidal field windings; these configurations can be elongated up to $\kappa \geq 3$, maintaining intrinsic vertical stability. They should exhibit robust stability at high normalized β_N [4, 5] and very high values of volume averaged beta (values of $\langle \beta \rangle$ up to 4% in ohmic discharges and up to 12% in additionally heated discharges have been obtained in the START experiment [2] and values of $\langle \beta \rangle$ up to 40% are expected in the next generation of spherical tori). They should have increased stability for kink and tearing modes; as a matter of fact the START experiment indicates the possible absence of disruptions in spherical tori. They are endowed with an omnigeneous ($|B| \approx \text{constant}$) region on the outboard

side of the torus (also at zero β value) and correspondingly show a minimal volume averaged geodesic curvature of the lines of force $\langle \kappa_s R \rangle$; toroidal plasma rotation can be easily imparted and should result in strong $\mathbf{E} \times \mathbf{B}$ shear stabilization of microinstabilities: these properties along with the high plasma density, the high current density and the strong shaping indicate the possibility of high confinement. The small major radius R , the high toroidal component of the diamagnetic current and the large bootstrap current at high β reduce the power requirements for non-inductive current drive, which could be accomplished by direct current helicity injection [6]. All these characteristics lead to a promising extrapolation to compact volumetric neutron sources [7] and to small reactors [8].

Furthermore, spherical tori offer the diagnostic advantage of enhancing the detachment of the constant toroidal current density j_ϕ surfaces from the flux ψ surfaces with respect to conventional aspect ratio tokamaks. This should in principle allow a much

better separation of the poloidal beta β_p from the internal self-inductance $l_i/2$ by the equilibrium magnetic measurements alone [9] and should even permit an accurate estimate of the j_ϕ profile, when the shape of the measured pressure profile is added [10] to the magnetic data. However, the reduced space allowed for magnetic sensors near the central conductor in spherical tokamaks, and the possibility of producing flux core spheromak configurations [6] without a central conductor, raise the question of what it is possible to measure if magnetic probes are not present in the cavity of a spherical torus and, furthermore, the question about which non-magnetic data must be added to the data given by the magnetic probes around the plasma sphere.

In order to answer these questions, a number of configurations considered for the SPHERA proposal [11], which is a spherical torus experiment at the moment under study at CR-ENEA Frascati, all endowed with a double or single null separatrix, are calculated by a predictive equilibrium code [12], as illustrated in Section 2.

Section 3 gives details of the expression for the flux function in spherical co-ordinates (r is radius, θ is colatitude and ϕ is azimuth), which is [13], in terms of index-1, order- n spherical harmonics $\sin\theta P_n^1(\cos\theta)$ and of the internal M_n^i and external M_n^e spherical multipolar moments,

$$\psi = \sum_{n=1}^{\infty} [M_n^i(r)r^{-n} + M_n^e(r)r^{n+1}] \sin\theta P_n^1(\cos\theta).$$

In Section 4, the fluxes and fields produced by the predictive equilibrium calculations are analysed in terms of the spherical multipolar moments obtained from simulated magnetic measurements located only upon a sphere $r = r_{pr}$ surrounding the spherical plasma.

Section 5 deals with the attempt to reconstruct the plasma boundary using constant spherical multipolar moments. Whereas the positions of the X points as well as the shape of the outboard plasma boundary ($\psi = \psi_X$) turn out to be very well determined, the reconstructed inboard plasma boundary deviates from the true boundary even near the X point and, furthermore, the total plasma current I_p remains undetermined. This is obviously due to the radial behaviour of $M_n^i(r)$ and $M_n^e(r)$, which cannot be derived from magnetic measurements external to the plasma sphere.

Section 6 shows that by fixing the plasma inboard boundary on the equatorial plane ($r = r_{in}$, $\theta = \pi/2$)

from non-magnetic measurements (e.g., spectroscopy), a spherical iterative equilibrium reconstruction can be obtained. The constraint $\psi(r_{in}) = \psi_X$ is added to the constraints of matching the odd internal spherical multipoles $M_n^i(r_{pr})$ (with $n = 1, 3, 5, 7$) in an iterative solution of the Grad-Shafranov equation, based on a spherical geometry. The plasma pressure is expressed by the functional form $p(\psi) = p_1\psi^\lambda$ (with $0.5 < \lambda < 1.5$), and the parametric form $f^2(\psi) = f_1\psi^{-1} + f_2\psi^{0.1} + f_3\psi^1 + f_4\psi^2$ is used for the squared diamagnetic current. The five unknowns $[p_1, f_1, f_2, f_3, f_4]$ are determined by the data $[r_{in}, M_1^i(r_{pr}), M_3^i(r_{pr}), M_5^i(r_{pr}), M_7^i(r_{pr})]$. The external spherical multipoles $M_n^e(r_{pr})$ (with $n = 1, 2, \dots, 7$) are used as boundary conditions, whereas the even internal spherical multipoles $M_n^i(r)$ (for $n = 2, 4, 6$ they are zero in up-down symmetric plasmas) are renormalized, at each iteration step, in order to match the measured $M_n^i(r_{pr})$ at the boundary.

The convergence of the spherical reconstructive equilibrium code is extremely fast, and Section 7 shows that the j_ϕ profile is extremely well reconstructed in the peaked, flat and hollow cases. Even the profiles of plasma pressure and diamagnetic current are reconstructed with good accuracy. The effect of an uncertainty $\pm\delta r_{in}$ on the spectroscopic identification of the plasma inboard boundary on the equatorial plane produces a large uncertainty in the reconstructed profiles of plasma pressure and diamagnetic current, but a more limited error on the reconstruction of the current density profile.

Finally, Section 8 is devoted to conclusions.

2. THE SPHERICAL TORUS AND THE PROBLEM WITH MAGNETIC MEASUREMENTS

In the case of an axisymmetric plasma, where the vector potential \mathbf{A} can be expressed through the scalar flux function $\psi = 2\pi R A_\phi$ (R is the distance from the symmetry axis), assuming static MHD equilibrium ($\nabla p = \mathbf{j} \times \mathbf{B}$, $\mu_0 \mathbf{j} = \nabla \times \mathbf{B}$), the Grad-Shafranov equation [14] is obtained in the cylindrical co-ordinates (R, Z, ϕ) ,

$$\frac{\partial^2 \psi}{\partial R^2} + \frac{\partial^2 \psi}{\partial Z^2} - \frac{1}{R} \frac{\partial \psi}{\partial R} = -2\pi\mu_0 R j_\phi(R, \psi) \quad (1)$$

and its current density source is specified as

$$j_\phi(R, \psi) = 2\pi R \frac{dp(\psi)}{d\psi} + \frac{\mu_0}{4\pi R} \frac{df^2(\psi)}{d\psi} \quad (2)$$

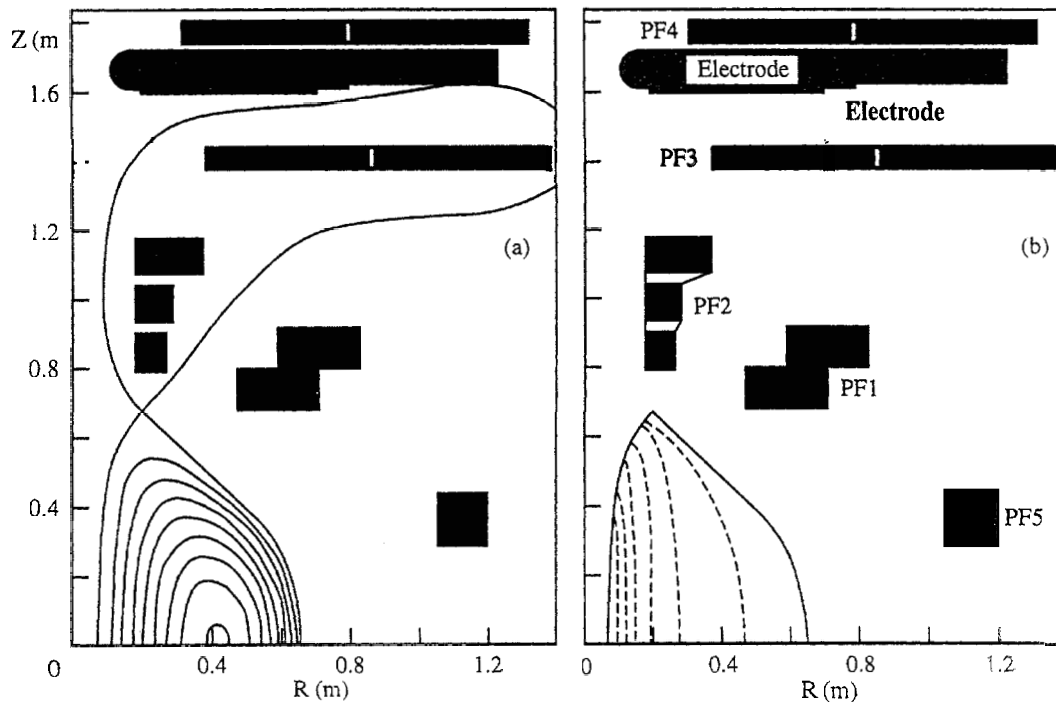


FIG. 1. Predictive equilibrium for SPHERA with toroidal current $I_p = 2.7$ MA; pinch current $I_e = 0.38$ MA, which means $B_{T0} = 0.212$ T at $R = 0.36$ m; $p(\psi) = \psi^{1.1}$ and $f^2(\psi) = \psi^{1.1}$; $\beta_p = 0.07$, which raises B_T to 1.05 T. The poloidal field coils are shown in black, whereas the upper electrode feeding the pinch current I_e is shown in grey. (a) Contour map of flux function ψ , (b) contour map of toroidal current density j_ϕ .

where $p(\psi)$ is the kinetic plasma pressure and $f(\psi)$ the diamagnetic plasma current.

In a spherical torus the extreme toroidicity should help in the task of the experimental equilibrium reconstruction, as the cylindrical degeneracy, which is due to the coincidence between constant toroidal current density j_ϕ surfaces and constant flux ψ surfaces in a cylinder, is completely removed by the large excursion of the factors R and $1/R$ in the current density source (2). The enhancement in the detachment of the j_ϕ surfaces from the ψ surfaces, which is obtained in spherical tori, with respect to conventional aspect ratio tokamaks, is illustrated in Fig. 1. It refers to a predictive equilibrium calculation for the SPHERA experiment proposal.

The SPHERA experiment proposal is to test an ultralow aspect ratio tokamak (ULART) [15], where the central conductor is substituted by a current carrying plasma, typically a stabilized screw pinch, fed by two electrodes placed on the polar caps of the plasma sphere. Such a configuration has been investigated under the name 'bumpy Z pinch' [16] or 'flux

core spheromak' [3, 17]. In its most advanced scenario, SPHERA tries to overcome the two main difficulties of the ULART concept: to avoid neutron damage to the central conductor [18] and to sustain the ULART configuration, in the absence of inductive current drive, through DC helicity injection, obtained by driving the plasma current I_e along the lines of force of the central screw pinch. The feasibility of such a configuration is very difficult to treat theoretically: a dedicated experiment could have great importance for proving this solution.

A configuration very similar to that of SPHERA has been obtained on TS-3 at Tokyo University [19]. The configuration set-up on TS-3 is a flux core spheromak smaller than SPHERA by a factor of 5 to 6 in linear dimensions. The toroidal plasma has been formed starting only from the current driven between the external electrodes of two plasma guns. The magnetic field measurements confirm the establishment of a flux core spheromak, whose formation from the longitudinal electrode current is attributed to a kink mode, which is able to convert the magnetic

Table I. Main Parameters of the Three Phases of the Proposed SPHERA Experiment

	SPHERA-RF	SPHERA-HI	SPHERA
R (m)	0.415	0.385	0.36
a (m)	0.305	0.295	0.29
A	1.36	1.3	≤ 1.25
I_p (MA)	3	1	≤ 2.7
B_{T0} (T)	2.3	0.33	0.212
$\langle\beta\rangle$ (%)	2-4	22	24
Auxiliary heating ^a	NBI (95 keV, 4 MW), LHCD (8 GHz, 3 MW), ECRH (140 GHz, 1.5 MW)	HICD (>2 MW), NBI (95 keV, 4 MW)	HICD (>4 MW), NBI (95 keV, 4 MW)
Pulse length (s)	1.5	>15	>15

^a NBI, neutral beam injection.

flux from poloidal to toroidal. A compression experiment has also been successfully undertaken [20]. The configuration has been maintained for about 100 μ s, i.e. tens of Alfvén times, before becoming unstable probably owing to a tilt instability caused by the excessive compression [15].

The most advanced scenario of SPHERA with the central screw pinch must be prepared through preliminary simpler scenarios, which are ULART experiments with a central conductor. Two scenarios with central conductor can be envisaged: SPHERA-RF with lower hybrid current drive (LHCD), electron cyclotron resonant heating (ECRH) and NBI and SPHERA-HI with helicity injection current drive (HICD), where a large divertor region allows the study of helicity injection, even in circumstances where powers of a few tens of megawatts should be required on the electrodes. The central rod alone, among all other windings, could be a cryogenic liquid nitrogen conductor. The main parameters of the three experimental phases of SPHERA are shown in Table I.

In particular, in the flux core spheromak configuration, where a current carrying plasma replaces the central conductor, magnetic probes cannot be present in the hole of the spherical torus and must be limited to loop voltages and poloidal pick-up coils around the plasma sphere (Fig. 2). Even in the other scenarios with a central rod, the limited available space (which must host the conductor, the cryogenic cooling channels and an outer vacuum sealing) could prevent the insertion of magnetic probes in the central hole of the spherical torus. This raises the question about what can be measured if magnetic probes are not present

in the cavity of a spherical torus and, furthermore, the question about which non-magnetic data must be added to the data of magnetic probes around a plasma sphere.

In order to answer these questions the three scenarios SPHERA, SPHERA-RF and SPHERA-HI, the first two endowed with a double null separatrix and the last one with a single null separatrix, have been calculated using the ODIN predictive equilibrium code [12, 21]. This code is based upon the expansion of the flux function in toroidal multipolar moments and is able to produce spherical torus equilibria simultaneously down to an aspect ratio $A = 1.2$ and up to an elongation $\kappa = 3$, when run in free boundary mode. The ODIN code is based on a toroidal co-ordinate mesh, which is made of non-concentric circular cross-section tori; the mesh boundary necessary for including a spherical plasma is many times greater than the plasma region and encompasses all the poloidal field coils. Thus, the predictive equilibria are achieved by using the toroidal multipolar expansion up to the very high poloidal number $m = 11$ and by accounting for the flux from all the poloidal field coils through elliptic integrals.

Other predictive equilibrium calculations are shown in Fig. 3, where a variety of plasmas envisaged for the proposed SPHERA experiments are considered. Figure 3(a) shows a larger aspect ratio $A = 1.5$ calculated for the formation and compression scenario of SPHERA, before reaching the final configuration of Fig. 1; Fig. 3(b) shows a reversed shear profile for SPHERA-RF and Fig. 3(c) a single null configuration for SPHERA-HI.

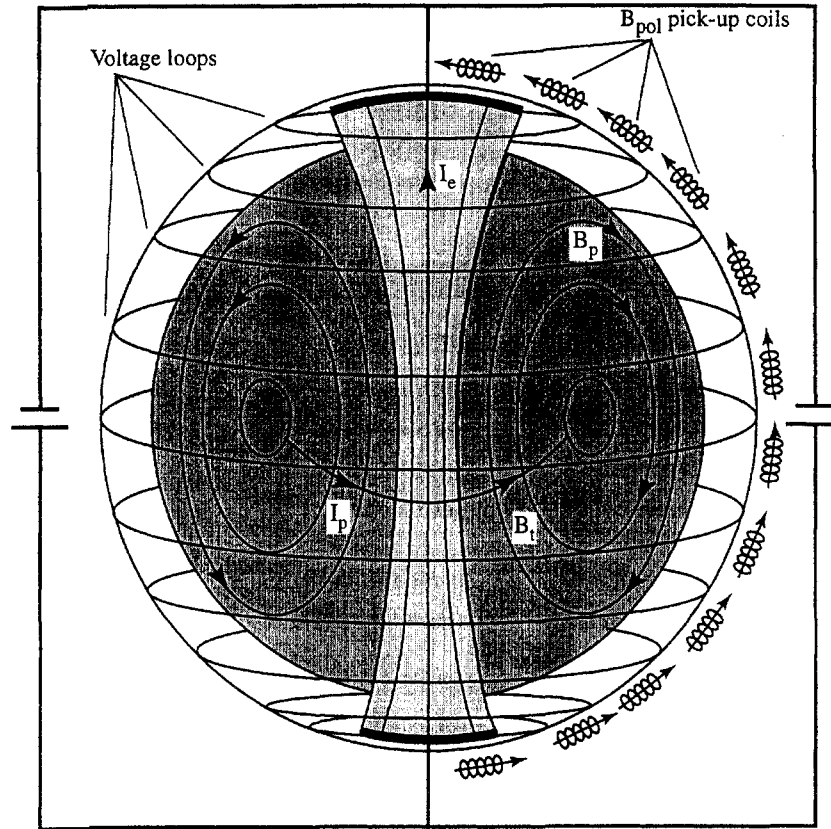


FIG. 2. Flux core spheromak configuration, where a current carrying plasma replaces the central conductor: magnetic probes cannot be present in the cavity of the spherical torus and must be limited to loop voltages and poloidal pick-up coils around the plasma sphere.

However, the reconstructive version of the ODIN equilibrium code [12] cannot be used for diagnosing spherical torus equilibria, as it is based upon the truncation to the low toroidal multipolar order $m = 3$. This has forced us to set up an equilibrium reconstruction code based on spherical co-ordinates [22], which are in any event the most natural co-ordinates for treating spherical tori.

3. SPHERICAL MULTIPOLAR EXPANSION

The spherical co-ordinates are a well known standard choice in mathematical physics [22]. In the axisymmetrical case, when the vector potential \mathbf{A} is expressed through the scalar flux function $\psi = 2\pi R A_\phi$, the homogeneous magnetostatic vector equation $\nabla^2 \mathbf{A} = 0$ becomes, in spherical co-ordinates,

$$\frac{\partial^2 \psi}{\partial r^2} + \frac{\sin \theta}{r^2} \frac{\partial}{\partial \theta} \left(\frac{1}{\sin \theta} \frac{\partial \psi}{\partial \theta} \right) = 0 \quad (3)$$

and admits a decomposition in the form

$$\psi(r, \theta) = \sum_{n=1}^{\infty} (M_n^i r^{-n} + M_n^e r^{n+1}) \sin \theta P_n^1(\cos \theta) \quad (4)$$

where the constants M_n^i and M_n^e depend on the conditions at the boundaries of the currentless domain (included between two concentric spheres) in which (3) holds. The functions $P_n^1(\cos \theta)$ are index-1, order- n Legendre polynomials [22]. An additional term ($M_0 r \cos \theta$) is neglected here, as it represents an unphysical radial cylindrical symmetric magnetic field, diverging like $1/R$. The additional arbitrary constant is such that $\psi = 0$ on the symmetry axis $\theta = 0, \pi$.

The inhomogeneous magnetostatic vector equation $\nabla^2 \mathbf{A} = -\mu_0 \mathbf{j}$, in the case of axial symmetry, becomes [13],

$$\frac{\partial^2 \psi}{\partial r^2} + \frac{\sin \theta}{r^2} \frac{\partial}{\partial \theta} \left(\frac{1}{\sin \theta} \frac{\partial \psi}{\partial \theta} \right) = -2\pi \mu_0 r \sin \theta j_\phi(r, \theta) \quad (5)$$

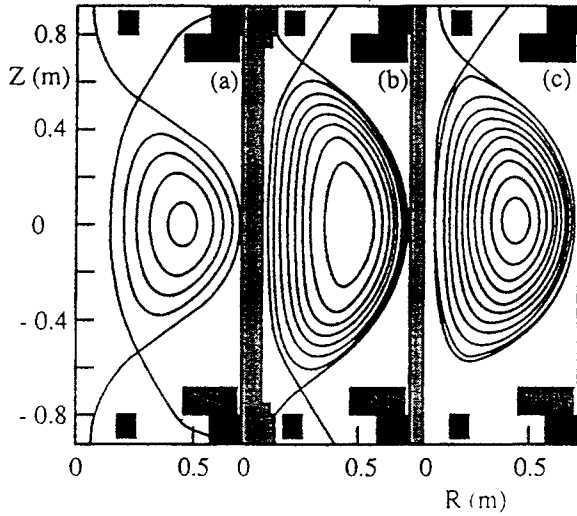


FIG. 3. Predictive equilibria for SPHERA. (a) Contour map of flux function ψ for SPHERA during formation and compression with toroidal current $I_p = 0.345$ MA, pinch current $I_e = 0.38$ MA, $p(\psi) = \psi^{1.3}$ and $f^2(\psi) = \psi^{1.3}$, and $\beta_p = 0.1$. (b) Contour map of ψ for SPHERA-RF with $I_p = 3.0$ MA, $B_{T0} = 2.3$ T at $R = 0.36$ m; $p(\psi)$ and $f^2(\psi)$ are polynomials able to produce a hollow j_ϕ profile and $\beta_p = 0.25$, which raises B_T to 2.6 T. (c) Contour map of ψ for SPHERA-HI with $I_p = 1.0$ MA, $B_{T0} = 0.33$ T at $R = 0.36$ m, $p(\psi) = \psi^{1.3}$ and $f^2(\psi) = \psi^{1.3}$, and $\beta_p = 0.1$. The poloidal field coils are the same as those shown in full in Fig. 1. The central conductors are shown in grey in (b) and (c). The electrodes are the same as those shown in Fig. 1 in (a), they are absent in (b) and they are present in both the upper separatrix tails in the single null configuration shown in (c).

when (5) is solved over the entire space, with the regulatory condition $\lim_{|r| \rightarrow \infty} |\nabla\psi| = 0$, the flux function admits, in spherical co-ordinates, a decomposition very similar to (4),

$$\psi(r, \theta) = \sum_{n=1}^{\infty} [M_n^i(r)r^{-n} + M_n^e(r)r^{n+1}] \sin\theta P_n^1(\cos\theta) \quad (6)$$

where the functions $M_n^i(r)$ and $M_n^e(r)$ are respectively the internal and external spherical multipolar moments of order n associated with the current density j_ϕ .

The expression for the internal spherical multipolar moments is evaluated as an integral of the toroidal current density $j_\phi(r_0, \theta_0)$ which flows inside the sphere with radius r ,

$$M_n^i(r) = \int_0^r dr_0 \int_0^\pi d\theta_0 \frac{\pi\mu_0 \sin\theta_0 P_n^1(\cos\theta_0)}{n(n+1)} r_0^{n+2} j_\phi(r_0, \theta_0). \quad (7)$$

For the external spherical multipolar moments, the integral is over the toroidal current density, which flows outside the sphere with radius r ,

$$M_n^e(r) = \int_r^\infty dr_0 \int_0^\pi d\theta_0 \frac{\pi\mu_0 \sin\theta_0 P_n^1(\cos\theta_0)}{n(n+1)} r_0^{-n+1} j_\phi(r_0, \theta_0). \quad (8)$$

The poloidal field is

$$\begin{aligned} \mathbf{B} &= \nabla \times \mathbf{A} = \frac{\nabla\psi \times \mathbf{e}_\phi}{2\pi r \sin\theta} \\ &= \frac{\partial\psi/\partial\theta}{2\pi r^2 \sin\theta} \mathbf{e}_r - \frac{\partial\psi/\partial r}{2\pi r \sin\theta} \mathbf{e}_\theta. \end{aligned}$$

As the radial derivatives of internal and external multipolar moments are connected by

$$dM_n^i(r)/dr = -r^{2n+1} dM_n^e(r)/dr \quad (9)$$

in full analogy with the case of the toroidal multipolar moments [23], one can show that the radial derivatives of the spherical multipolar moments are not relevant to the calculation of the poloidal magnetic field,

$$\begin{aligned} B_r(r, \theta) &= -\frac{1}{2\pi} \sum_{n=1}^{\infty} [M_n^i(r)r^{-n-2} \\ &\quad + M_n^e(r)r^{n-1}] n(n+1) P_n^0(\cos\theta) \end{aligned} \quad (10)$$

$$\begin{aligned} B_\theta(r, \theta) &= \frac{1}{2\pi} \sum_{n=1}^{\infty} [nM_n^i(r)r^{-n-2} \\ &\quad - (n+1)M_n^e(r)r^{n-1}] P_n^1(\cos\theta) \end{aligned} \quad (11)$$

where $P_n^0(\cos\theta)$ are index-0, order- n Legendre polynomials [22].

4. ANALYSIS OF SPHERICAL TORUS EQUILIBRIA IN SPHERICAL CO-ORDINATES

Magnetic measurements can be located, as shown in Fig. 2, on a half-meridian circle lying upon a sphere ($r = r_{pr}$) that surrounds the spherical plasma and does not contain any poloidal field coils. Referring to Fig. 1 and to (7) and (8), it is apparent that the currents flowing in the poloidal field coils generate the external multipolar moments $M_n^e(r_{pr})$, and that the current flowing in the plasma generates the internal multipolar moments $M_n^i(r_{pr})$, provided that r_{pr} is inside the coils. The multipolar expansion (6) is the solution to the local Cauchy problem of determining the flux function ψ when the flux and its normal

derivative on the surface $r = r_{\text{pr}}$ are known. Conversely, it is clear that the measurement of the flux ψ at $r = r_{\text{pr}}$, designated by $\psi^{\text{pr}}(\theta)$, and of the poloidal field B_θ tangential to the sphere $r = r_{\text{pr}}$, designated by $B_\theta^{\text{pr}}(\theta)$, can determine both the internal and the external multipolar expansion. By using (6) and (11), as well as the orthogonality property of associated Legendre functions

$$\int_0^\pi \sin \theta P_p^1(\cos \theta) P_q^1(\cos \theta) d\theta = \frac{2}{2p+1} \frac{(p+1)!}{(p-1)!} \delta_{pq}$$

the value of the spherical multipolar moments can be derived as

$$M_n^i(r_{\text{pr}}) = \frac{r_{\text{pr}}^n}{2n} \int_0^\pi \psi^{\text{pr}}(\theta) P_n^1(\cos \theta) d\theta + \frac{\pi r_{\text{pr}}^{n+2}}{n(n+1)} \int_0^\pi B_\theta^{\text{pr}}(\theta) \sin \theta P_n^1(\cos \theta) d\theta \quad (12)$$

$$M_n^e(r_{\text{pr}}) = \frac{r_{\text{pr}}^{-n-1}}{2(n+1)} \int_0^\pi \psi^{\text{pr}}(\theta) P_n^1(\cos \theta) d\theta - \frac{\pi r_{\text{pr}}^{-n+1}}{n(n+1)} \int_0^\pi B_\theta^{\text{pr}}(\theta) \sin \theta P_n^1(\cos \theta) d\theta. \quad (13)$$

The values of $\psi^{\text{pr}}(\theta)$ and of $B_\theta^{\text{pr}}(\theta)$ have been calculated from the predictive equilibrium code on one hundred points, equally spaced in co-latitude θ , on a half-meridian circle ($0 \leq \theta \leq \pi$) located on the sphere $r = r_{\text{pr}} = 0.75$ m (full curves in Fig. 4).

As the poloidal field coils PF1 and PF2 (Fig. 1(b)) are quite near to the measurement contour, their field

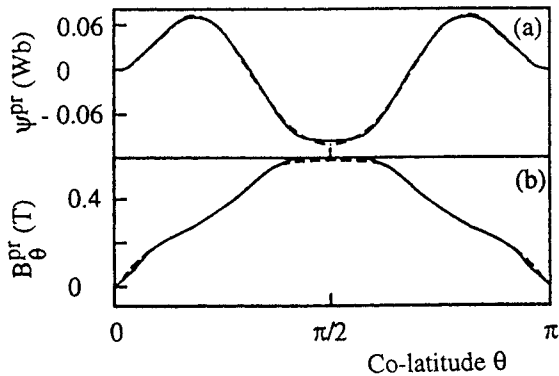


FIG. 4. The SPHERA experiment with toroidal current $I_p = 2.7$ MA, pinch current $I_e = 0.38$ MA, same parameters as those in Fig. 1: (a) predictive equilibrium calculation (full curve) and description by spherical harmonics truncated to $n = 7$ (dashed curve) for flux measurement $\psi^{\text{pr}}(\theta)$, (b) predictive equilibrium calculation (full curve) and description by spherical harmonics truncated to $n = 7$ (dashed curve) for poloidal field measurement $B_\theta^{\text{pr}}(\theta)$ tangential to the sphere $r = r_{\text{pr}} = 0.75$ m.

is described by an excessively high number ($n \geq 11$) of multipolar moments. The measurement of such high orders of spherical multipoles would not be feasible in an experiment. On the other hand, a truncated measurement up to the order $n = 7$ should be feasible: in an up-down symmetric spherical torus the non-zero internal spherical multipolar moments are only the odd ones, $n = 1, 3, 5, 7$. The $n = 7$ internal spherical moment expresses the triangular deformation of the current density inside the plasma and this triangular multipolar component is easily measured in conventional large aspect ratio tokamaks [12]. The accuracy of the truncation is cured by assuming the currents flowing in PF1 and PF2 as being perfectly known: the $\psi^{\text{PF}}(\theta)$ and $B_\theta^{\text{PF}}(\theta)$ contributions they produce on the measurement contour are calculated separately through elliptic integrals. The remaining configuration can be well described by a series of spherical harmonics truncated to $n = 7$,

$$\psi^{\text{pr}}(\theta) = \psi^{\text{PF}}(\theta) + \sum_{n=1}^7 [M_n^i(r_{\text{pr}}) r_{\text{pr}}^{-n} + M_n^e(r_{\text{pr}}) r_{\text{pr}}^{n+1}] \sin \theta P_n^1(\cos \theta) \quad (14)$$

$$B_\theta^{\text{pr}}(\theta) = B_\theta^{\text{PF}}(\theta) + \frac{1}{2\pi} \sum_{n=1}^7 [n M_n^i(r_{\text{pr}}) r_{\text{pr}}^{-n-2} - (n+1) M_n^e(r_{\text{pr}}) r_{\text{pr}}^{n-1}] P_n^1(\cos \theta). \quad (15)$$

The result of the spherical multipolar analysis is shown as dashed curves in Fig. 4, which represents the field and fluxes calculated on $r = r_{\text{pr}}$ through the series (14) and (15) truncated to $n = 7$; the effect of PF1 and PF2 is summed back after (12) and (13) have determined $M_n^i(r_{\text{pr}})$ and $M_n^e(r_{\text{pr}})$. Fits with similar accuracy ($\Delta\psi/\psi \leq 5\%$, $\Delta B_\theta/B_\theta \leq 3\%$) are obtained when other predictive equilibria, such as those shown in Fig. 3, are analysed in terms of spherical co-ordinates.

5. RECONSTRUCTION OF THE PLASMA BOUNDARY

The simplest attempt is that of reconstructing the plasma shape by a series of constant spherical multipolar moments, truncated to $n = 7$,

$$\psi^{\text{vac}}(r, \theta) = \psi^{\text{PF}}(r, \theta) + \sum_{n=1}^7 [M_n^i(r_{\text{pr}}) r^{-n} + M_n^e(r_{\text{pr}}) r^{n+1}] \sin \theta P_n^1(\cos \theta). \quad (16)$$

This attempt is quite clearly doomed to failure: the radial behaviours of $M_n^i(r)$ and $M_n^e(r)$ are far

from being constant and obviously remain unknown from magnetic measurements external to the plasma sphere. However, it is the first step in the direction of an equilibrium reconstruction.

The flux surfaces of (16) are explored by searching for a null point of the associated poloidal field, which is expressed by a series of constant spherical multipolar moments, truncated to $n = 7$,

$$B_{\theta}^{\text{vac}}(r, \theta) = B_{\theta}^{\text{PF}}(\theta) + \frac{1}{2\pi} \sum_{n=1}^7 [nM_n^i(r_{\text{pr}})r^{-n-2} - (n+1)M_n^e(r_{\text{pr}})r^{n-1}]P_n^1(\cos \theta) \quad (17)$$

$$B_r^{\text{vac}}(r, \theta) = B_r^{\text{PF}}(\theta) - \frac{1}{2\pi} \sum_{n=1}^7 [M_n^i(r_{\text{pr}})r^{-n-2} + M_n^e(r_{\text{pr}})r^{n-1}]n(n+1)P_n^0(\cos \theta). \quad (18)$$

The plasma boundary is labelled by the value $\psi^{\text{vac}} = \psi_X$ taken at the null point. Whereas the positions of the X points as well as the shape of the outboard plasma boundary (Fig. 5) turn out to be very well determined (an error of 2% of the outboard radius of the plasma sphere $r = R_{\text{sph}}$), the reconstructed inboard plasma boundary deviates from the true boundary by 5% of R_{sph} as soon as the first 15

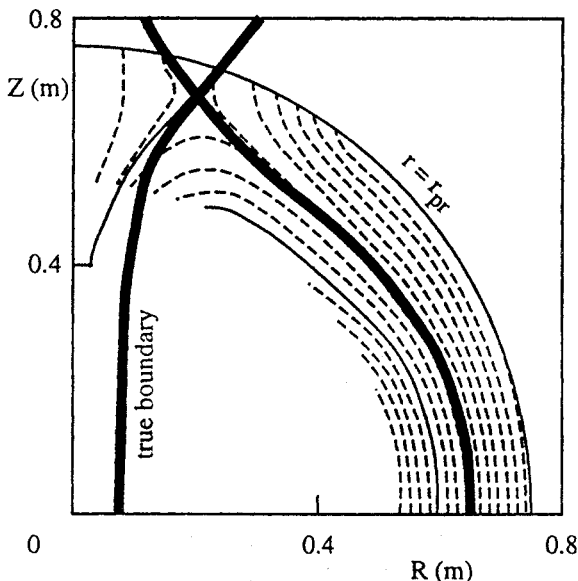


FIG. 5. The SPHERA experiment with toroidal current $I_p = 2.7$ MA, pinch current $I_e = 0.38$ MA and the same parameters as those in Fig. 1. Boundary of predictive equilibrium calculation (heavy curves) and constant spherical multipolar moment reconstruction of flux surfaces (light curves), obtained by measurements situated upon the sphere $r = r_{\text{pr}} = 0.75$ m. The series of spherical harmonics is truncated to the order $n = 7$.

to 20% of R_{sph} is entered, and even the total plasma current I_p cannot be determined. Similar results are also obtained for the other predictive equilibria shown in Fig. 3, where the larger aspect ratio case $A = 1.5$ shown in Fig. 3(a) exhibits the larger deviation of the internal boundary.

The two main quantities that remain undetermined, i.e. the toroidal plasma current I_p and the plasma inboard boundary on the equatorial plane ($r = r_{\text{in}}, \theta = \pi/2$), are indeed connected. By substituting (6) into (5) one derives the following expression for the toroidal plasma current density in terms of the internal spherical multipolar moments:

$$j_{\phi}(r, \theta) = \frac{1}{2\pi\mu_0} \sum_{n=1}^{\infty} (2n+1)r^{-n-2} \times \frac{\partial M_n^i(r)}{\partial r} P_n^1(\cos \theta). \quad (19)$$

This simple expression allows the evaluation of the total toroidal plasma current inside the ULART in terms of the odd ordered internal spherical multipolar moments,

$$I_p = -\frac{1}{\pi\mu_0} \sum_{\text{odd } n=1}^{\infty} (2n+1) \times \left(M_n^i(r_{\text{pr}}) + (n+1) \int_{r_{\text{in}}}^{r_{\text{pr}}} M_n^i(r)r^{-n-2} dr \right). \quad (20)$$

This expression shows that in order to evaluate precisely the total toroidal plasma current it is necessary to know both the position of r_{in} as well as the radial behaviour of the odd ordered internal spherical multipolar moments.

6. EQUILIBRIUM RECONSTRUCTION IN SPHERICAL GEOMETRY

The connection between the plasma inboard boundary on the equatorial plane ($r = r_{\text{in}}, \theta = \pi/2$) and the total plasma current I_p can therefore be exploited only through a full equilibrium reconstruction. As the data obtained from magnetic probes around the plasma sphere are not sufficient for this purpose, one can in addition fix r_{in} from non-magnetic measurements (e.g., visible spectroscopy): experimental data from X point plasmas in the START spherical torus show that, when viewed by a high speed videocamera in visible light, the plasma boundary appears especially sharp on the inboard side [24].

In the case of a spherical torus axisymmetric plasma, the Grad-Shafranov equation, expressed in spherical co-ordinates, is (5) and the current density source is specified as

$$j_\phi(r \sin \theta, \psi) = 2\pi r \sin \theta \frac{dp(\psi)}{d\psi} + \frac{\mu_0}{4\pi r \sin \theta} \frac{df^2(\psi)}{d\psi} \quad (21)$$

where $p(\psi)$ is the kinetic plasma pressure and $f(\psi)$ the diamagnetic plasma current. The problem of the equilibrium reconstruction is to start from the boundary conditions, i.e. the spectrum of the spherical multipolar moments and the plasma inboard boundary on the equatorial plane, and to work back to an estimate on the $p(\psi)$ and $f^2(\psi)$ functions. Fitting the plasma pressure by the functional form $p(\psi) = p_1 \psi^\lambda$ (with $0.5 < \lambda < 1.5$) and the squared diamagnetic current by $f^2(\psi) = f_1 \psi^\alpha + f_2 \psi^\beta + f_3 \psi^\gamma + f_4 \psi^\delta$ (with $\alpha = -1$, $\beta = 0.1$, $\gamma = 1$, $\delta = 2$ as a standard choice) allows the description of a large set of current density profiles, including hollow and peaked ones.

In an experimental equilibrium reconstruction a fit of the measured pressure profile [10] would replace the monomial expression $p_1 \psi^\lambda$. The choice of using four exponents for the squared diamagnetic current $f^2(\psi)$ (which cannot be directly measured) is forced by the truncation to $n = 7$ of the internal spherical multipolar moments. In the iterative solution of the Grad-Shafranov equation, the five unknowns $[p_1, f_1, f_2, f_3, f_4]$ are determined, together with ψ , by the data $[r_{\text{in}}, M_1^i(r_{\text{pr}}), M_3^i(r_{\text{pr}}), M_5^i(r_{\text{pr}}), M_7^i(r_{\text{pr}})]$.

The iteration is started from a reasonable guess for the ψ function and for the five coefficients $[\tilde{p}_1, \tilde{f}_1, \tilde{f}_2, \tilde{f}_3, \tilde{f}_4]$. The iterative process runs as follows: the values of the tentative internal multipolar moments at the edge of the mesh are calculated from the ψ , $[\tilde{p}_1, \tilde{f}_1, \tilde{f}_2, \tilde{f}_3, \tilde{f}_4]$ evaluated at the previous iteration step, as

$$\begin{aligned} \tilde{M}_n^i(r_{\text{pr}}) = & \sum_{j,k} \{ S_n^i(j, k) \lambda \tilde{p}_1 \psi_{j,k}^{\lambda-1} \\ & + I_n^i(j, k) [\alpha \tilde{f}_1 \psi_{j,k}^{\alpha-1} + \beta \tilde{f}_2 \psi_{j,k}^{\beta-1} \\ & + \gamma \tilde{f}_3 \psi_{j,k}^{\gamma-1} + \delta \tilde{f}_4 \psi_{j,k}^{\delta-1}] \}. \end{aligned} \quad (22)$$

To carry out the calculation inside the plasma, a mesh (r_j, θ_k) , with $0 < r_j \leq r_{\text{pr}}$ and $j = 1, \dots, 60$, $0 \leq \theta_k \leq \pi$ and $k = 1, \dots, 60$,

based on spherical co-ordinates and evenly spaced ($\Delta r = \text{constant}$, $\Delta \theta = \text{constant}$), has been set up. The multipolar expansion of the Grad-Shafranov current density (21) leads to the definition of the following purely geometrical mesh functions $S_n^i(j, k)$, $S_n^e(j, k)$, $I_n^i(j, k)$ and $I_n^e(j, k)$:

$$S_n^{\{i,e\}}(j, k) = (\Delta r \Delta \theta) \frac{2\pi^2 \mu_0}{n(n+1)} \sin^2 \theta_k P_n^1(\cos \theta_k) \begin{cases} r_j^{n+3} \\ r_j^{-n+2} \end{cases} \quad (23)$$

$$I_n^{\{i,e\}}(j, k) = (\Delta r \Delta \theta) \frac{\mu_0^2}{4n(n+1)} P_n^1(\cos \theta_k) \begin{cases} r_j^{n+1} \\ r_j^{-n} \end{cases}. \quad (24)$$

A set of correction factors $[\tilde{p}'_1, \tilde{f}'_1, \tilde{f}'_2, \tilde{f}'_3, \tilde{f}'_4]$ is evaluated by matching the $\tilde{M}_n^i(r_{\text{pr}})$, evaluated at the edge of the mesh at the previous iteration step, with the measured internal odd-ordered spherical multipoles $M_n^i(r_{\text{pr}})$ (derived from (12) and (13) with $n = 1, 3, 5, 7$):

$$\begin{aligned} M_n^i(r_{\text{pr}}) = & \tilde{p}'_1 \left(\lambda \tilde{p}_1 \sum_{j,k} S_n^i(j, k) \psi_{j,k}^{\lambda-1} \right) \\ & + \tilde{f}'_1 \left(\alpha \tilde{f}_1 \sum_{j,k} I_n^i(j, k) \psi_{j,k}^{\alpha-1} \right) \\ & + \tilde{f}'_2 \left(\beta \tilde{f}_2 \sum_{j,k} I_n^i(j, k) \psi_{j,k}^{\beta-1} \right) \\ & + \tilde{f}'_3 \left(\gamma \tilde{f}_3 \sum_{j,k} I_n^i(j, k) \psi_{j,k}^{\gamma-1} \right) \\ & + \tilde{f}'_4 \left(\delta \tilde{f}_4 \sum_{j,k} I_n^i(j, k) \psi_{j,k}^{\delta-1} \right) \end{aligned} \quad (25)$$

for $n = 1, 3, 5, 7$. The flux surfaces are explored by searching for the null point of the poloidal field associated with the ψ evaluated at the previous iteration step, and the value ψ_X of the flux function at the null point is computed (the vacuum value derived from (16), $\psi_X = \psi_{\text{vac}}$, is used at the first iteration). The constraint $\psi(r_{\text{in}}, \pi) = \psi_X$ is matched multiplying the external moments $\tilde{M}_n^e(r_{\text{in}})$, evaluated at the inboard plasma boundary at the previous iteration step, by the correction factors $[\tilde{p}'_1, \tilde{f}'_1, \tilde{f}'_2, \tilde{f}'_3, \tilde{f}'_4]$,

$$\begin{aligned}
 \psi_X = & \psi^{\text{PF}}(r_{\text{in}}, \pi) + \sum_{n=1}^7 [r_{\text{in}}^{n+1} P_n^1(0) M_n^e(r_{\text{pr}})] \\
 & + \tilde{p}'_1 \left[\lambda \tilde{p}_1 \sum_{n=1}^7 \left(r_{\text{in}}^{n+1} P_n^1(0) \sum_{\substack{m,k \\ r_m > r_{\text{in}}}} S_n^e(m, k) \psi_{m,k}^{\lambda-1} \right) \right] \\
 & + \tilde{f}'_1 \left[\alpha \tilde{f}_1 \sum_{n=1}^7 \left(r_{\text{in}}^{n+1} P_n^1(0) \sum_{\substack{m,k \\ r_m > r_{\text{in}}}} I_n^e(m, k) \psi_{m,k}^{\alpha-1} \right) \right] \\
 & + \tilde{f}'_2 \left[\beta \tilde{f}_2 \sum_{n=1}^7 \left(r_{\text{in}}^{n+1} P_n^1(0) \sum_{\substack{m,k \\ r_m > r_{\text{in}}}} I_n^e(m, k) \psi_{m,k}^{\beta-1} \right) \right] \\
 & + \tilde{f}'_3 \left[\gamma \tilde{f}_3 \sum_{n=1}^7 \left(r_{\text{in}}^{n+1} P_n^1(0) \sum_{\substack{m,k \\ r_m > r_{\text{in}}}} I_n^e(m, k) \psi_{m,k}^{\gamma-1} \right) \right] \\
 & + \tilde{f}'_4 \left[\delta \tilde{f}_4 \sum_{n=1}^7 \left(r_{\text{in}}^{n+1} P_n^1(0) \sum_{\substack{m,k \\ r_m > r_{\text{in}}}} I_n^e(m, k) \psi_{m,k}^{\delta-1} \right) \right]
 \end{aligned} \tag{26}$$

which is derived from (14), taking into account the fact that all the internal spherical moments are zero for $r \leq r_{\text{in}}$, as no toroidal plasma current flows inside the innermost sphere $r \leq r_{\text{in}}$. The system of Eqs (25) and (26) is solved as a determined system of five equations in five unknowns.

Then the radial behaviour of the internal spherical multipolar moments is evaluated as

$$\begin{aligned}
 M_n^i(r_j) = & \tilde{p}'_1 \left(\lambda \tilde{p}_1 \sum_{\substack{m,k \\ r_m < r_j}} S_n^i(m, k) \psi_{m,k}^{\lambda-1} \right) \\
 & + \tilde{f}'_1 \left(\alpha \tilde{f}_1 \sum_{\substack{m,k \\ r_m < r_j}} I_n^i(m, k) \psi_{m,k}^{\alpha-1} \right) \\
 & + \tilde{f}'_2 \left(\beta \tilde{f}_2 \sum_{\substack{m,k \\ r_m < r_j}} I_n^i(m, k) \psi_{m,k}^{\beta-1} \right) \\
 & + \tilde{f}'_3 \left(\gamma \tilde{f}_3 \sum_{\substack{m,k \\ r_m < r_j}} I_n^i(m, k) \psi_{m,k}^{\gamma-1} \right) \\
 & + \tilde{f}'_4 \left(\delta \tilde{f}_4 \sum_{\substack{m,k \\ r_m < r_j}} I_n^i(m, k) \psi_{m,k}^{\delta-1} \right).
 \end{aligned} \tag{27}$$

The renormalization of the even ordered internal $M_n^i(r)$ (with $n = 2, 4, 6$) during the iterations is simply obtained, step by step, by forcing their values outside the plasma to be equal to the measured ones $M_n^i(r_{\text{pr}})$, after the matching of the odd ordered $M_n^i(r)$ has been performed through the determined system (25) and (26).

Thereafter the radial behaviour of the external spherical multipolar moments is evaluated,

$$\begin{aligned}
 M_n^e(r_j) = & M_n^e(r_{\text{pr}}) + \tilde{p}'_1 \left(\lambda \tilde{p}_1 \sum_{\substack{m,k \\ r_m > r_j}} S_n^e(m, k) \psi_{m,k}^{\lambda-1} \right) \\
 & + \tilde{f}'_1 \left(\alpha \tilde{f}_1 \sum_{\substack{m,k \\ r_m > r_j}} I_n^e(m, k) \psi_{m,k}^{\alpha-1} \right) \\
 & + \tilde{f}'_2 \left(\beta \tilde{f}_2 \sum_{\substack{m,k \\ r_m > r_j}} I_n^e(m, k) \psi_{m,k}^{\beta-1} \right) \\
 & + \tilde{f}'_3 \left(\gamma \tilde{f}_3 \sum_{\substack{m,k \\ r_m > r_j}} I_n^e(m, k) \psi_{m,k}^{\gamma-1} \right) \\
 & + \tilde{f}'_4 \left(\delta \tilde{f}_4 \sum_{\substack{m,k \\ r_m > r_j}} I_n^e(m, k) \psi_{m,k}^{\delta-1} \right).
 \end{aligned} \tag{28}$$

The measured external spherical multipoles $M_n^e(r_{\text{pr}})$ (with $n = 1, 2, \dots, 7$) are used as boundary conditions. The new approximation to ψ is calculated as usual by (6), and this distribution, along with the product of the previous $[\tilde{p}_1, \tilde{f}_1, \tilde{f}_2, \tilde{f}_3, \tilde{f}_4]$, respectively, times the newly determined $[\tilde{p}'_1, \tilde{f}'_1, \tilde{f}'_2, \tilde{f}'_3, \tilde{f}'_4]$ are fed back into the first step of the iteration (22) until the difference in ψ between two successive iterations is less than a specified fraction of ψ over all the mesh. After the solution has reached convergence, using the determined $[p_1, f_1, f_2, f_3, f_4]$ and the ψ distribution, it is straightforward to calculate the most important quantities connected with the equilibrium [25], i.e. the poloidal beta β_p , the internal self-inductance $l_i/2$ and the paramagnetism μ_i [12]. The convergence of the spherical reconstructive equilibrium code is extremely fast, usually only five to six iterations are required to reach a precision of $\Delta\psi/\psi = 10^{-4}$.

The absence of a mesh generator and the speed of convergence of semianalytical deterministic Grad-Shafranov solvers [10, 12] are their main advantages with respect to finite element variational least squares

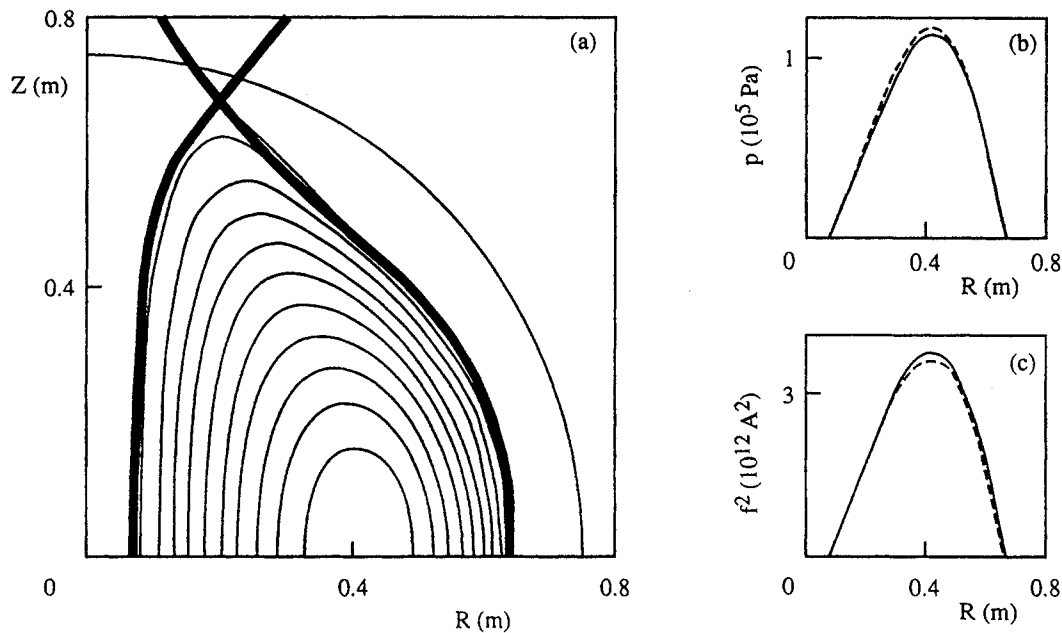


FIG. 6. The SPHERA experiment with toroidal current $I_p = 2.7$ MA, pinch current $I_e = 0.38$ MA and $\beta_p = 0.07$. (a) Contour map of flux function ψ from equilibrium reconstruction (light curves) compared with plasma boundary from predictive equilibrium calculation of Fig. 1 (heavy curves); the measurement contour is situated on the sphere $r = r_{pr} = 0.75$ m. (b) Profile of plasma pressure $p(\psi)$ as a function of R on the equatorial plane from the predictive equilibrium calculation (full curve) and from the equilibrium reconstruction (dashed curve). (c) As (b) but for the square of the diamagnetic plasma current $f^2(\psi)$.

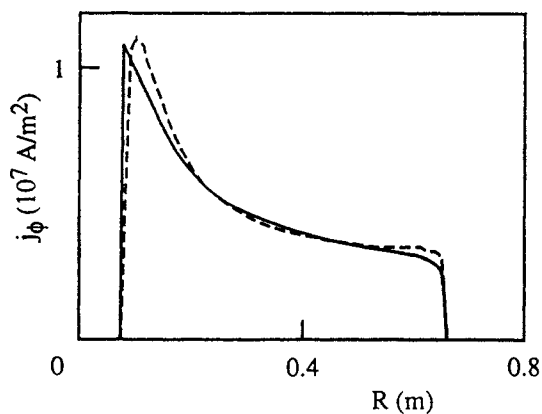


FIG. 7. The SPHERA experiment with toroidal current $I_p = 2.7$ MA, pinch current $I_e = 0.38$ MA and $\beta_p = 0.07$. Profile of toroidal current density j_ϕ as a function of R on the equatorial plane from the predictive equilibrium calculation (full curve) and from the equilibrium reconstruction (dashed curve).

fit methods [26, 27], which have been widely employed in the analysis of tokamak experiments. The deterministic nature of the solver here presented, which also helps with the speed of the calculation, is, however, a disadvantage as far as the flexibility is concerned: as a matter of fact the least squares fit methods [26, 27] have shown a very broad capability of incorporating a variety of diagnostic information.

7. RESULTS OF THE EQUILIBRIUM RECONSTRUCTION IN SPHERICAL GEOMETRY

The first case examined by the equilibrium reconstruction code is the full current scenario of SPHERA, whose predictive equilibrium is shown in Fig. 1. It is an ULART configuration with aspect ratio $A = 1.25$, for which the plasma inboard boundary on the equatorial plane is $r_{in} = 7.3$ cm and the plasma outboard boundary is $R_{sph} = 65.2$ cm. The safety factor profile is such that on the magnetic axis $q_0 \approx 1.1$ and at the edge $q_{95} \approx 2$. Figure 6(a)

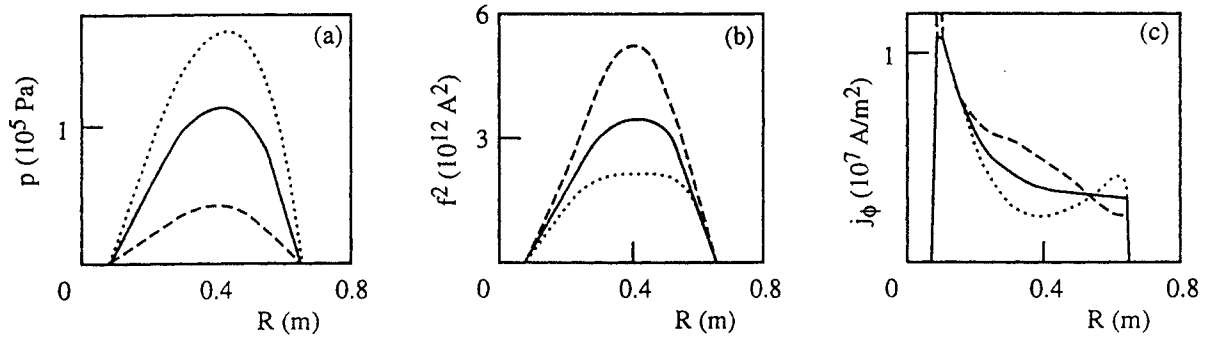


FIG. 8. The SPHERA experiment with toroidal current $I_p = 2.7$ MA, pinch current $I_e = 0.38$ MA and $\beta_p = 0.07$. Effect of the uncertainty of the spectroscopic identification of the plasma inboard boundary on the equilibrium reconstruction: the dashed curves refer to $r_{in} = 7.3 + 0.5$ cm, the dotted curves to $r_{in} = 7.3 - 0.5$ cm and the full curves to $r_{in} = 7.3$ cm. (a) Profile of the reconstructed plasma pressure $p(\psi)$, (b) profile of the reconstructed square of the diamagnetic plasma current $f^2(\psi)$ and (c) profile of the reconstructed toroidal current density j_ϕ as functions of R on the equatorial plane.

Table II. SPHERA with Toroidal Current $I_p = 2.7$ MA, Pinch Current $I_e = 0.38$ MA and $\beta_p = 0.07$

(Macroscopic quantities as calculated from predictive equilibrium and from reconstructive equilibrium, including the uncertainty on the plasma inboard boundary r_{in} : outboard boundary R_{sph} , toroidal plasma current I_p , poloidal beta β_p , internal self-inductance $l_i/2$ and paramagnetism μ_i)

	r_{in} (cm)	R_{sph} (cm)	I_p (MA)	β_p	$l_i/2$	μ_i
Predictive	7.3	65.2	2.70	0.070	0.110	-0.330
Reconstructive	7.3 + 0.5	64.4	2.56	0.130	0.092	-0.280
Reconstructive	7.3	64.4	2.72	0.073	0.104	-0.324
Reconstructive	7.3 - 0.5	64.4	2.88	0.022	0.116	-0.362

shows the result of the equilibrium reconstruction, obtained by fixing the exponent of the plasma pressure $p(\psi) = p_1\psi^\lambda$ to the value used in the predictive calculation, $\lambda = 1.1$. The error on the total plasma current is less than 1%, 20 kA over $I_p = 2.7$ MA; the error in the position of the plasma boundary is at most 2% of R_{sph} (owing to the truncation to $n = 7$ spherical harmonics); the error on the poloidal beta is 0.003 over $\beta_p = 0.07$ and the error on the internal self-inductance is 0.006 over $l_i/2 = 0.11$. Even the profiles of plasma pressure and of diamagnetic current are reconstructed within a few per cent, Figs 6(b) and (c). The j_ϕ profile is extremely well reconstructed, as shown in Fig. 7. The accuracy of the safety factor profile reconstruction is such that on the magnetic axis $\delta q_0/q_0 \approx 10\%$.

The effect of an uncertainty $\pm\delta r_{in}$ upon the spectroscopic identification of the plasma inboard boundary on the equatorial plane is assessed in Fig. 8,

where an error $\delta r_{in} = \pm 0.5$ cm over $r_{in} = 7.3$ cm produces a large uncertainty on the reconstructed profiles of plasma pressure and diamagnetic current, but a more limited error on the reconstruction of the current density profile. Table II summarizes the effect of an uncertainty $\pm\delta r_{in}$ upon the main macroscopic plasma quantities. The uncertainty introduced on the q_0 value is $\delta q_0/q_0 = \pm 11\%$.

The effect of the uncertainty connected with the choice of the exponent of the plasma pressure $p(\psi) = p_1\psi^\lambda$ in the range $0.5 < \lambda < 1.5$ is shown in Fig. 9 and turns out to be almost null on the reconstruction of the current density profile and quite small even on the reconstructed profiles of plasma pressure and diamagnetic current. Also the main macroscopic plasma quantities are unaffected by variations of λ in the range $0.5 < \lambda < 1.5$.

The second case examined is the larger aspect ratio $A = 1.5$ (Fig. 3(a)) calculated for the formation

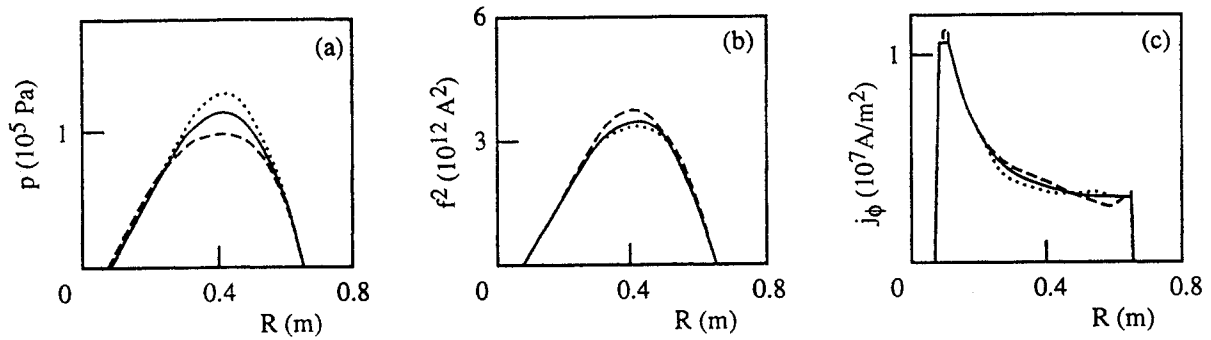


FIG. 9. The SPHERA experiment with toroidal current $I_p = 2.7$ MA, pinch current $I_e = 0.38$ MA and $\beta_p = 0.07$. Effect of the uncertainty of the exponent λ of the plasma pressure $p(\psi) = p_1 \psi^\lambda$ on the equilibrium reconstruction: the dashed curves refer to $\lambda = 1.5$, the full curves to $\lambda = 1.1$ and the dotted curves to $\lambda = 0.5$. (a) Profile of the reconstructed plasma pressure $p(\psi)$, (b) profile of the reconstructed square of the diamagnetic plasma current $f^2(\psi)$ and (c) profile of the reconstructed toroidal current density j_ϕ as functions of R on the equatorial plane.

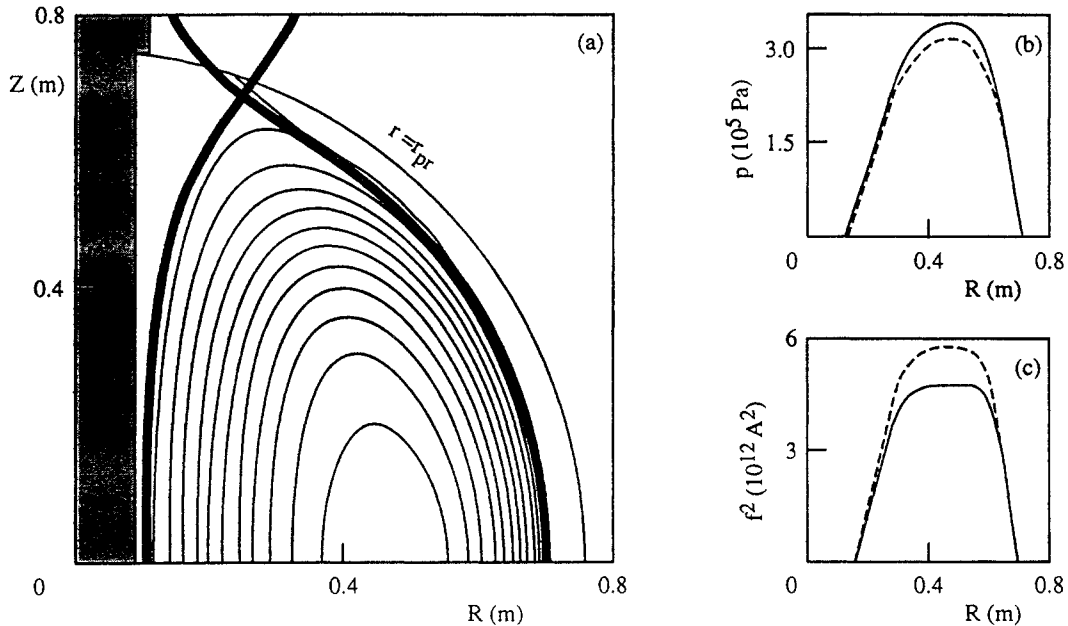


FIG. 10. The SPHERA-RF experiment with $I_p = 3.0$ MA, $B_{T0} = 2.3$ T at $R = 0.36$ m and $\beta_p = 0.25$, which raises B_T to 2.6 T. (a) Contour map of flux function ψ from equilibrium reconstruction (light curves) compared with plasma boundary from the predictive equilibrium calculation of Fig. 3(b) (heavy curves); the measurement contour is situated on the sphere $r = r_{pr} = 0.75$ m, the central conductor is shown in grey. (b) Profile of plasma pressure $p(\psi)$ as a function of R from the predictive equilibrium calculation (full curve) and from the equilibrium reconstruction (dashed curve), (c) as (b) but for the square of the diamagnetic plasma current $f^2(\psi)$.

and compression scenario, before reaching the final configuration. The plasma inboard boundary on the equatorial plane is $r_{in} = 14.3$ cm and the plasma outboard boundary is $R_{sph} = 69.9$ cm. The safety factor profile is such that on the magnetic axis $q_0 \approx 1.0$ and at the edge $q_{95} \approx 2.5$. The error on the total plasma current is about 3%, 11 kA over $I_p = 345$ kA; the

error in the position of the plasma boundary is at most 1% of R_{sph} (owing to the truncation to $n = 7$ spherical harmonics); the error on the poloidal beta is 0.02 over $\beta_p = 0.10$ and the one on the internal self-inductance is 0.035 over $l_i/2 = 0.23$. The accuracy of the safety factor profile reconstruction is such that on the magnetic axis $\delta q_0/q_0 \approx 17\%$ and the

Table III. SPHERA-RF with $I_p = 3.0$ MA, $B_{T0} = 2.3$ T at $R = 0.36$ m and $\beta_p = 0.25$

(Macroscopic quantities as calculated from predictive equilibrium and from reconstructive equilibrium, including the uncertainty on the plasma inboard boundary r_{in} : outboard boundary R_{sph} , toroidal plasma current I_p , poloidal beta β_p , internal self-inductance $l_i/2$ and paramagnetism μ_i)

	r_{in} (cm)	R_{sph} (cm)	I_p (MA)	β_p	$l_i/2$	μ_i
Predictive	10.9	70.5	3.00	0.250	0.160	-0.380
Reconstructive	10.9 + 0.5	69.7	2.88	0.284	0.179	-0.374
Reconstructive	10.9	69.7	2.88	0.241	0.184	-0.410
Reconstructive	10.9 - 0.5	69.7	3.12	0.170	0.195	-0.468

uncertainty introduced by an error $\delta r_{in} = \pm 0.5$ cm on the q_0 value is $\delta q_0/q_0 = \pm 25\%$.

The third case considered is a reversed shear profile for SPHERA-RF (Fig. 3(b)) with $q_{min} \approx 3$ and $q_{95} \approx 7$. The plasma inboard boundary on the equatorial plane is $r_{in} = 10.9$ cm and the plasma outboard boundary is $R_{sph} = 70.5$ cm. Figure 10(a) shows the result of the equilibrium reconstruction, obtained by fixing the exponent of the plasma pressure $p(\psi) = p_1 \psi^\lambda$ to the intermediate value $\lambda = 1$; in this case, the predictive equilibrium was generated by polynomial functions for both $p(\psi)$ and $f^2(\psi)$.

The error on the total plasma current is about 4%, 120 kA over $I_p = 3.0$ MA; the error on the position of the plasma boundary is at most 1% of R_{sph} (owing to the truncation to $n = 7$ spherical harmonics); the error on the poloidal beta is 0.01 over $\beta_p = 0.25$ and that on the internal self-inductance is 0.024 over $l_i/2 = 0.16$. The profiles of plasma pressure and of diamagnetic current are reconstructed with a good accuracy, Figs 10(b) and (c).

Table III summarizes the effect of an uncertainty $\pm \delta r_{in}$ in the spectroscopic identification of the plasma inboard boundary upon the main macroscopic plasma quantities.

The hollow j_ϕ profile, shown in Fig. 11, is extremely well reconstructed. The accuracy of the safety factor profile reconstruction is such that at the minimum of the hollow q profile $\delta q_{min}/q_{min} \approx 6\%$ and the uncertainty introduced by an error $\delta r_{in} = \pm 0.5$ cm on the q_{min} value is $\delta q_{min}/q_{min} = \pm 6\%$.

The effect of the values of β_p and $l_i/2$ on the accuracy of the equilibrium reconstruction has been explored. At low values of internal self-inductance $l_i/2 \approx 0.2$ (which are the most typical of spherical

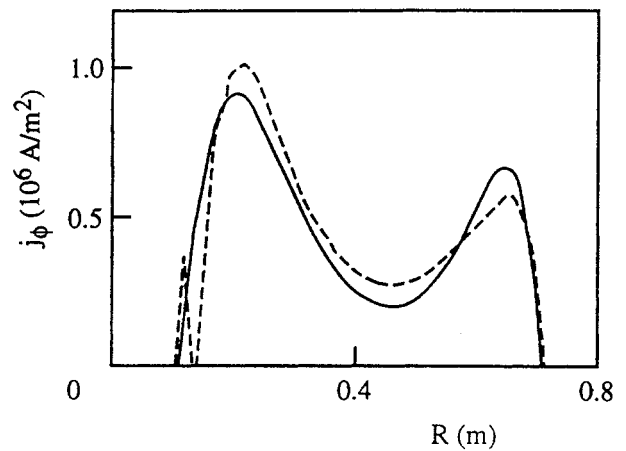


FIG. 11. The SPHERA-RF experiment with $I_p = 3.0$ MA, $B_{T0} = 2.3$ T at $R = 0.36$ m and $\beta_p = 0.25$. Profile of toroidal current density j_ϕ as a function of R on the equatorial plane from the predictive equilibrium calculation (full curve) and from the equilibrium reconstruction (dashed curve).

tori), the accuracy of the reconstruction increases monotonically with the value of β_p : as an example at $A \approx 1.3$, the error on the determination of β_p and $l_i/2$ decreases from $\delta \beta_p/\beta_p \approx \delta(l_i/2)/(l_i/2) \approx \pm(4-5)\%$ for $\beta_p = 0.07$ to $\delta \beta_p/\beta_p \approx \delta(l_i/2)/(l_i/2) \approx \pm(1-2)\%$ for $\beta_p = 0.50$. Even the effect of the uncertainty upon β_p and $l_i/2$ introduced by an inaccuracy $\delta r_{in} = 5\%$ in the spectroscopic identification of the plasma inboard boundary decreases from $\delta \beta_p/\beta_p \approx \delta(l_i/2)/(l_i/2) \approx \pm(40-70)\%$ for $\beta_p = 0.07$ to $\delta \beta_p/\beta_p \approx \delta(l_i/2)/(l_i/2) \approx \pm(5-15)\%$ for $\beta_p = 0.50$. The beneficial effect of β_p is due to the increase of the Shafranov shift, which makes the external field and fluxes more sensitive to the internal distributions of pressure and current.

On the other hand, the increase of self-inductance decreases the accuracy of the equilibrium reconstruction: as an example at $A \approx 1.3$ and $\beta_p = 0.50$, the error on the determination of β_p and $l_i/2$ decreases from $\delta\beta_p/\beta_p \approx \delta(l_i/2)/(l_i/2) \approx \pm(1-2)\%$ for $l_i/2 = 0.26$ to $\delta\beta_p/\beta_p \approx \delta(l_i/2)/(l_i/2) \approx \pm(5-10)\%$ for $l_i/2 = 0.67$. Even the effect of the uncertainty upon β_p and $l_i/2$ introduced by an inaccuracy $\delta r_{in} = \pm 5\%$ in the spectroscopic identification of the plasma inboard boundary increases from $\delta\beta_p/\beta_p \approx \delta(l_i/2)/(l_i/2) \approx \pm(5-15)\%$ for $l_i/2 = 0.26$ to $\delta\beta_p/\beta_p \approx \delta(l_i/2)/(l_i/2) \approx \pm(10-40)\%$ for $l_i/2 = 0.67$. The negative effect of $l_i/2$ is due to the increase of the current density flowing on large aspect ratio flux surfaces. It has to be remarked, however, that values of $l_i/2 = 0.67$ correspond in spherical tori to extremely peaked current density profiles, such as those having a safety factor $q_0 \approx 1.0$ on the magnetic axis with $q_{95} \approx 12$. Furthermore, the uncertainty in the q_0 value remains quite limited, $\delta q_0/q_0 \approx \pm 10\%$, even allowing for an inaccuracy $\delta r_{in}/r_{in} = \pm 5\%$ or for an uncertainty in the exponent λ of the plasma pressure $p(\psi) = p_1 \psi^\lambda$, which introduces an uncertainty in the value of the plasma pressure at the magnetic axis, $\delta p(\psi_{axis})/p(\psi_{axis}) \approx \pm 50\%$.

The effect of the uncertainties upon the absolute values of the magnetic measurements can be estimated to be less than $\pm 1\%$ [10]; this error should be negligible as it is much less than the multipole truncation error ($\pm(3-5)\%$) that is considered here. A further effect introduced by the mechanical limitations to the positions of the measuring probes cannot be ascertained in general, but must be dealt with on the basis of the detailed design of the load assembly of the spherical torus experiment.

8. CONCLUSIONS

In spherical tori the cylindrical degeneracy, which is due to the coincidence between constant toroidal current density j_ϕ surfaces and constant flux ψ surfaces, is completely removed. This should help in the task of the experimental equilibrium reconstruction from magnetic measurements. However, the reduced space available near the central conductor in spherical tokamaks and the possibility of producing flux core spheromak configurations without a central conductor could prevent the insertion of magnetic probes in the central cavity of spherical tori.

A variety of spherical torus configurations, all endowed with a double or single null separatrix, in

a range of aspect ratios $1.2 < A < 1.5$ and with peaked, flat and hollow j_ϕ profiles have been calculated by a predictive equilibrium code. The fluxes and fields produced by the predictive equilibrium calculations have been analysed in terms of the spherical multipolar moments obtained from simulated magnetic probe measurements located only upon the sphere $r = r_{pr}$ surrounding the spherical plasma. The attempt to reconstruct the spherical plasma boundary through constant spherical multipolar moments gives the obvious result that the positions of the X points as well as the shape of the outboard plasma boundary ($\psi = \psi_X$) are very well determined, but it is impossible to reconstruct the inboard plasma boundary and even the total plasma current I_p remains undetermined.

As the data obtained from magnetic probes around the plasma sphere are not sufficient for attempting a full plasma equilibrium reconstruction, one has to determine, in addition, from non-magnetic measurements (e.g., visible spectroscopy) the plasma inboard boundary on the equatorial plane $r = r_{in}$. The constraint $\psi(r_{in}, \pi) = \psi_X$ is added to the constraints of matching the odd internal spherical multipoles $M_n^i(r_{pr})$ (with $n = 1, 3, 5, 7$) in an iterative solution of the Grad-Shafranov equation, based on a spherical geometry. The plasma pressure is expressed by the function $p(\psi) = p_1 \psi^\lambda$ (with $0.5 < \lambda < 1.5$) and the parametric form

$$f^2(\psi) = f_1 \psi^{-1} + f_2 \psi^{0.1} + f_3 \psi^1 + f_4 \psi^2$$

is used for the squared diamagnetic current. The five unknowns $[p_1, f_1, f_2, f_3, f_4]$ are determined by the data $[r_{in}, M_1^i(r_{pr}), M_3^i(r_{pr}), M_5^i(r_{pr}), M_7^i(r_{pr})]$. The convergence of the spherical reconstructive equilibrium code is extremely fast, usually only five to six iterations are required to reach a precision of $\Delta\psi/\psi = 10^{-4}$.

The results of the spherical reconstruction are quite encouraging. The error on the total plasma current I_p is less than 1% at very low aspect ratio $A < 1.3$ and reaches 3% at $A = 1.5$. The error on the position of the plasma boundary is at most 2% of R_{sph} (owing to the truncation to $n = 7$ spherical harmonics), and the error on the poloidal beta β_p and that on the internal self-inductance $l_i/2$ at most 15%. Even the profiles of plasma pressure and of diamagnetic current are reconstructed to within a few per cent and, finally, the j_ϕ profile is extremely well reconstructed in peaked, flat and hollow cases.

The effect of the uncertainty connected with the choice of the exponent of the plasma pressure

$p(\psi) = p_1\psi^\lambda$, chosen in the range $0.5 < \lambda < 1.5$, turns out to be almost null on the reconstruction of the current density profile and quite small even on the reconstructed profiles of plasma pressure and diamagnetic current. Furthermore, the possibility of supplementing the shape of the measured pressure profile to an experimental equilibrium reconstruction should reduce this uncertainty.

The effect of an uncertainty $\pm\delta r_{in}$ upon the spectroscopic identification of the plasma inboard boundary on the equatorial plane produces a large uncertainty on the reconstructed profiles of plasma pressure and diamagnetic current and on the determination of β_p and of $l_i/2$, but a more limited error upon the total plasma current and upon the reconstruction of the current density profile. Therefore, the spectroscopic identification of the plasma inboard boundary is the most critical issue for the equilibrium reconstruction, when magnetic measurements cannot be inserted in the central cavity of a spherical torus.

REFERENCES

- [1] PENG, Y.-K.M., STRICKLER, D.J., Nucl. Fusion **26** (1986) 769.
- [2] SYKES, A., Plasma Phys. Control. Fusion **36** (1994) B93.
- [3] ROBINSON, D.C., in Tokamak Concept Improvements (Proc. Workshop Varenna, 1994), Editrice Compositori, Bologna (1994) 127.
- [4] TROYON, F., et al., Plasma Phys. Control. Fusion **26** (1984) 209.
- [5] HOLMES, J.A., et al., Phys. Fluids B **1** (1989) 358.
- [6] TAYLOR, J.B., TURNER, M.F., Nucl. Fusion **29** (1989) 219.
- [7] ABDOU, M.A., et al., in Plasma Physics and Controlled Nuclear Fusion Research 1994 (Proc. 15th Int. Conf. Seville, 1994), Vol. 2, IAEA, Vienna (1995) 733.
- [8] BUTTERY, R., et al., *ibid.*, p. 633.
- [9] FENEBERG, W., LACKNER, K., Nucl. Fusion **13** (1973) 549.
- [10] ALLADIO, F., MICOZZI, P., Nucl. Fusion **35** (1995) 305.
- [11] ALLADIO, F., CARDINALI, A., MICOZZI, P., PIERONI, L., Bull. Am. Phys. Soc. **41** (1996) 1405.
- [12] ALLADIO, F., CRISANTI, F., Nucl. Fusion **26** (1986) 1143.
- [13] ZAKHAROV, L.E., SHAFRANOV, V.D., Reviews of Plasma Physics, Vol. 12 (LEONTOVICH, M.A., Ed.), Consultants Bureau, New York (1986) 545.
- [14] SHAFRANOV, V.D., Sov. Phys.-JETP **6** (1958) 545.
- [15] YAMADA, M., POMPHREY, N., MORITA, A., ONO, Y., KATSURAI, M., Nucl. Fusion **36** (1996) 1210.
- [16] JENSEN, T.H., CHU, M.S., J. Plasma Phys. **25** (1980) 459.
- [17] TURNER, L., Phys. Fluids **27** (1984) 1677.
- [18] HENDER, T.C., et al., in Plasma Physics and Controlled Nuclear Fusion Research 1992 (Proc. 14th Int. Conf. Würzburg, 1992), Vol. 3, IAEA, Vienna (1993) 399.
- [19] AMEMIYA, N., HAYAKAWA, A., KATSURAI, M., J. Phys. Soc. Jpn. **60** (1991) 2632.
- [20] AMEMIYA, N., MORITA, A., KATSURAI, M., J. Phys. Soc. Jpn. **63** (1993) 1552.
- [21] ALLADIO, F., CRISANTI, F., MARINUCCI, M., MICOZZI, P., TANGA, A., Nucl. Fusion **31** (1991) 739.
- [22] MORSE, P.M., FESHBACH, H., Methods of Theoretical Physics, McGraw-Hill, New York (1953).
- [23] ALLADIO, F., MICOZZI, P., Phys. Plasmas **3** (1996) 72.
- [24] SYKES, A., et al., in Controlled Fusion and Plasma Physics (Proc. 22nd Eur. Conf. Bournemouth, 1995), Vol. 19C, Part III, European Physical Society, Geneva (1995) 117.
- [25] SHAFRANOV, V.D., Plasma Phys. **13** (1973) 757.
- [26] LAO, L.L., et al., Nucl. Fusion **25** (1985) 1611.
- [27] HIRSHMAN, S.P., et al., Phys. Plasmas **1** (1994) 2277.

(Manuscript received 18 February 1997)

Final manuscript accepted 9 September 1997)

E-mail address of F. Alladio:
alladio@frascati.enea.it

Subject classification: B0, Ti; C0, Ti; K0, Ti